Systematic Study of the Structures of Potassiated Tertiary Amino Acids: Salt Bridge Structures Dominate

Miriam K. Dray*β*,[†] Dirk Blunk,[†] Jos Oomens,[‡,||] Bing Gao,[§] Thomas Wyttenbach,[§] Michael T. Bowers,[§] and Mathias Schäfer*,[†]

Department of Chemistry, University of Cologne, Greinstraβe 4, 50939 Köln, Germany, FOM Institute for Plasmaphysics Rijnhuizen, Edisonbaan 14, NL-3439 MN Nieuwegein, The Netherlands, University of Amsterdam, Nieuwe Achtergracht 166, 1018WV Amsterdam, The Netherlands, and Department of Chemistry and Biochemistry, University of California, Santa Barbara, California

Received: April 2, 2009; Revised Manuscript Received: June 23, 2009

The gas-phase structures of a series of potassiated tertiary amino acids have been systematically investigated using infrared multiple photon dissociation (IRMPD) spectroscopy utilizing light generated by a free electron laser, ion mobility spectrometry (IMS), and computational modeling. The examined analytes comprise a set of five linear *N,N*-dimethyl amino acids derived from *N,N*-dimethyl glycine and three cyclic *N*-methyl amino acids including *N*-methyl proline. The number of methylene groups in either the alkyl chain of the linear members or in the ring of the cyclic members of the series is gradually varied. The spectra of the cyclic potassiated molecular ions are similar and well resolved, whereas the clear signals in the respective spectra of the linear analytes increasingly overlap with longer alkyl chains. Measured IRMPD spectra are compared to spectra calculated at the B3LYP/6-311++G(2d,2p) level of theory to identify the structures present in the experimental studies. On the basis of these experiments and calculations, all potassiated molecular ions of this series adopt salt bridge structures in the gas phase, involving bidentate coordination of the potassium cation to the carboxylate moiety. The assigned salt bridge structures are predicted to be the global minima on the potential energy surfaces. IMS cross-section measurements of the potassiated systems show a monotonic increase with growing system size, suggesting that the precursor ions adopt the same type of structure and comparisons between experimental and theoretical cross sections are consistent with salt bridge structures and the IRMPD results.

Introduction

Over the past several years, research on the elucidation of gas-phase ion structures has increased substantially, and ion mobility mass spectrometry,[1,2] infrared multiple photon dissociation (IRMPD) spectroscopy,[3,4] and collision-induced dissociation (CID)[5,6] combined with computational modeling[7−9] have successfully been applied. In particular complex molecular ions of natural amino acids[10−18] and oligopeptides[19−24] with different metal cations[25,26] (e.g., alkali[10−14,17,18,22] and alkaline earth metals[15,16]) have been investigated systematically. These studies provide ample evidence for the general trend that the formation of gas-phase salt bridges are explicitly favored with increasing size and charge of the metal ion.[10−16] The transition from canonical structures with a single formal charge site (charge solvation CS) to salt bridge (SB) structures is dependent on the gas-phase basicity of the amino acid[17,18] and was observed to occur at sodium for arginine, at potassium for *N*-methyl lysine, at cesium for serine, and perhaps around rubidium for threonine in the respective [amino acid + alkali metal]$^+$ molecular ion.[10−13] Armentrout et al. studied the gas-phase ion structure of proline and its four- and six-membered ring analogues with Li^+, Na^+, and K^+ with threshold CID and computational modeling and found that the complexes adopt salt bridge structures in the gas phase.[5]

SCHEME 1: Synthetic Tertiary Amino Acid Compounds C_n and R_n Derived from the Structures of *N,N*-Dimethyl Glycine (C_1) and *N*-Methyl Proline (R_1)

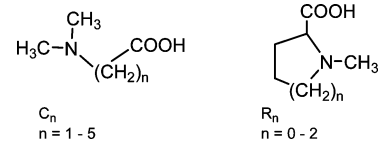

In the present work, gas-phase ion structures of a series of synthetic tertiary amino acids have been systematically investigated using the free electron laser for infrared experiments (FELIX), ion mobility spectrometry (IMS), and computational modeling. The series of synthetic compounds is derived from *N,N*-dimethyl glycine and *N*-methyl proline (Scheme 1). The number of methylene groups *n* in either the alkyl chain of the linear members (C_n) or in the ring of the cyclic members (R_n) of the series is gradually varied. The series of analytes possess a tertiary amino functionality with a substantial gas-phase basicity (for comparison: *N,N*-dimethyl ethyl amine = 929 kJ·mol^{-1}),[27] which is expected to lie in the range of lysine (lysine = 951 kJ·mol^{-1}).[27] All analytes are examined as potassiated molecular ions (Scheme 2).

It is reasonable to assume that throughout the series of molecules studied the gas-phase basicity of the tertiary amine group and the gas-phase acidity of the carboxylic functionality

* To whom correspondence should be addressed. Phone: (+49)221-470-3086. E-mail: mathias.schaefer@uni-koeln.de.
[†] University of Cologne.
[‡] FOM Institute for Plasmaphysics Rijnhuizen.
[||] University of Amsterdam.
[§] University of California, Santa Barbara.

10.1021/jp903036t CCC: $40.75
Published on Web 07/28/2009

SCHEME 2: Illustration of Possible Ion Structures Relevant for the Series of Potassiated Molecular Ions $[C_n + K]^+$ with $n = 1-5$ and $[R_n + K]^+$ $n = 0-2$ in the Gas Phase[a]

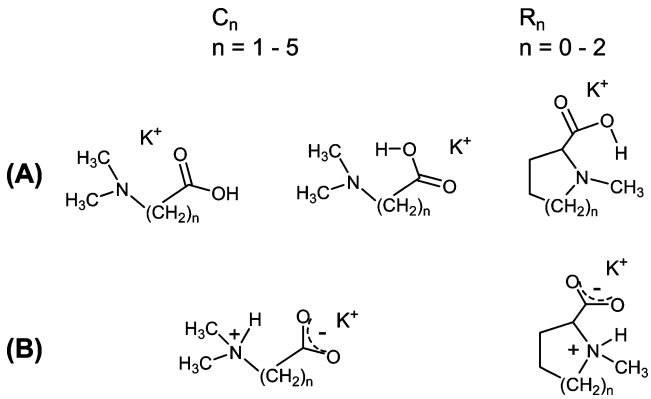

[a] (A) Canonical structures with a single formal charge site (charge solvation CS); (B) salt bridge SB structure.

are roughly constant and independent of the length of the alkyl chain. Given these assumptions, our intent is to probe the influence of subtle conformational changes of the molecules on the formation of gas-phase ion structures, in particular on the formation of salt bridges (Scheme 2).

Experimental Section

Materials. All solvents and chemicals used for the synthetic work were purchased from ABCR (Karlsruhe, Germany) or Acros Organics (Geel, Belgium) and were used without further purification.

Linear *N,N*-Dimethyl Amino Acids (C_n). The synthesis of the linear *N,N*-dimethylated amino acids C_4 and C_5 was accomplished by application of a modified Eschweiler−Clarke reaction.[28] The respective primary amino acid 5-amino pentanoic acid and 6-amino hexanoic acid was refluxed (11 h) in a mixture of 40% aqueous formaldehyde in formic acid. The products C_4 and C_5 were isolated as hydrochlorides by acidification with hydrochloric acid (conc.) and crystallization from acetone.

N,N-Dimethyl glycine (C_1) was purchased from TCI Europe (Eschborn, Germany). *N,N*-Dimethyl-3-amino propionic acid (C_2) and *N,N*-dimethyl-4-amino butanoic acid (C_3) were purchased from ABCR (Karlsruhe, Germany). All compounds were used without further purification.

Cyclic *N*-Methyl Amino Acids (R_n). *N*-Methyl proline (R_1) and its four- and six-membered ring analogues *N*-methyl-azetidine-2-carboxylic acid (R_0) and *N*-methyl pipecolic acid (R_2) (Scheme 1) were synthesized according to a procedure published by Aurelio et al.[29] The respective secondary amino acids proline, azetidine-2-carboxylic acid, and pipecolic acid were dissolved in methanol, and each solution was treated with an aqueous formaldehyde solution (40%) in the presence of 10% palladium on charcoal in a hydrogen atmosphere (1 bar, 16 h, 20 °C). The catalyst was removed by filtration and the respective product compounds R_0-R_2 were isolated as pure solids by removal of the solvent.

Mass Spectrometry and Photodissociation. A 4.7 T Fourier-transform ion cyclotron resonance (FTICR) mass spectrometer was used for the IRMPD experiments and has been described in detail elsewhere.[3,4,30,31] Tunable radiation for the photodissociation experiments is generated by the FELIX.[32] For the present experiments, spectra were recorded over the wavelength range from 1000 to 1800 cm^{-1}. Pulse energies were around 50 mJ per macropulse of 5 μs duration, although they fell off to about 20 mJ toward the blue edge of the scan range. The fwhm bandwidth of the laser was typically 0.5% of the central wavelength. Potassiated amino acids were formed by electrospray ionization using a Micromass Z-Spray source and a solution of 1 mM amino acid and 1−2 mM potassium chloride in 95%:5% MeOH/H_2O. Solution flow rates ranged from 15 to 30 μL/min, and the electrospray needle was generally held at a voltage of +3.2 kV. Ions were accumulated in a hexapole trap for about 2 s prior to being injected into the ICR cell via an rf octopole ion guide. Electrostatic switching of the dc bias of the octopole allows ions to be captured in the ICR cell without the use of a gas pulse, thus avoiding collisional heating of the ions.[31] All complex ions were irradiated for 3 s, corresponding to interaction with 15 macropulses.

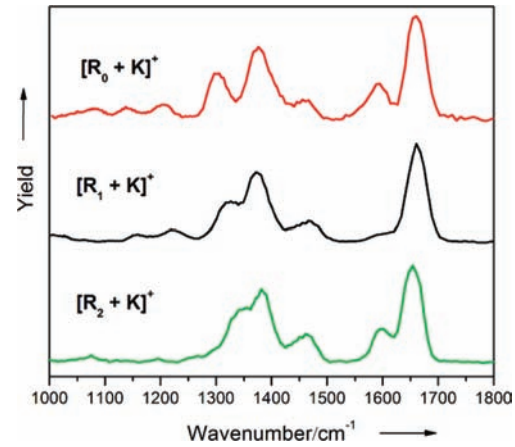

Figure 1. IRMPD spectra of potassiated molecular ions of cyclic *N*-methyl amino acids $[R_n + K]^+$, $n = 0, 1, 2$.

Activation of potassiated R_n and C_n complex ions $[C_n + K]^+$ and $[R_n + K]^+$ by infrared photons leads to the exclusive loss of the respective neutral amino acid ligand and the formation of the potassium cation at *m/z* 39. IRMPD spectra were recorded by monitoring the product ion formation (i.e., K^+ at *m/z* 39) over the 1000−1800 cm^{-1} range. The IRMPD yield was determined from the precursor (I_P) intensity and the intensity of the potassium product ion (I_{K+}) after laser irradiation at each frequency

$$\text{IRMPD yield} = I_{K+}/(I_P + I_{K+}) \quad (1)$$

The yield was normalized linearly with laser power to roughly account for the change in laser power as a function of photon energy (Figure 1).

IMS. The ion mobility experiments were carried out on a home-built high-resolution ion mobility mass spectrometer that has been previously described in detail.[33] Briefly, sample solutions were loaded into gold-coated borosilicate capillaries used for nano-ESI. Typical spray solutions had a sample concentration of ~100 μM (in 9:1 methanol:water) and a potassium acetate concentration of 2 mM. Ions generated in the ESI source were transferred into the vacuum via a capillary and focused in an ion funnel. The ion funnel also served as an ion trap, allowing conversion of the continuous ion beam into ion pulses by storing the ions for 100 ms and releasing them in short 80-μs pulses into a drift tube. A counter flow of helium buffer gas from the drift tube to the source chamber was maintained with a pressure differential of ~0.18 Torr between the two regions. This prevents air and unwanted neutral

TABLE 1: Relative Energies [kJ mol^{-1}] of All Conformers as Predicted by Theory for the Potassiated Molecular Ions [R_n + K]$^+$ with $n = 0-2$

	$[R_0 + K]^+$		$[R_1 + K]^+$		$[R_2 + K]^+$	
conformer	B3LYP[a]	MP2[a]	B3LYP[a]	MP2[b]	B3LYP[a]	MP2[b]
SB1	0	0	4.5	0	0.4	0
SB1a	–	–	0	6.5	0	0.9
SB2	31.5	27.6	37.2	34.8	–	–
SB3	34.7	30.1	37.8	34.9	18.0	17.2
SB4	–	–	–	–	11.7	11.1
CSz1	24.3	21.8	27.5	25.0	29.0	28.4
CSz1a	–	–	32.2	32.4	30.3	30.2
CSx1	27.3	24.0	37.2	36.8	26.9	24.4

[a] All structures are geometry optimized and have ZPE corrections calculated at the levels indicated: B3LYP = B3LYP/6-311++G(2d,2p); MP2 = MP2/6-311++G(2d,2p). All energy values are given in kJ mol^{-1}. [b] Single-point energies are calculated at the MP2/6-311++G(2d,2p)// B3LYP/6-311++G(2d,2p) level. All energy values are given in kJmol^{-1}.

TABLE 2: Relative Energies [kJ mol^{-1}] of All Conformers of [C_n + K]$^+$ with $n = 1-5$

	$[C_1 + K]^+$		$[C_2 + K]^+$		$[C_3 + K]^+$		$[C_4 + K]^+$		$[C_5 + K]^+$	
conformer	BLYP[a]	MP2[a]	B3LYP[a]	MP2[a]	B3LYP[a]	MP2[b]	B3LYP[a]	MP2[b]	B3LYP[a]	MP2[b]
SB1	0	0	0	0	0	0	0	0	0	0
SB2	–	–	–	–	–	–	–	–	5.7	10.5
SB3	–	–	54.6	15.7	–	–	–	–	–	–
SB4	–	–	55.4	15.7	–	–	–	–	–	–
SB5	25.5	6.6	–	–	–	–	–	–	–	–
CSx1	26.4	2.7	36.2	6.5	37.7	39.2	24.1	35.5	16.2	31.3
CSx2	45.7	7.0	52.7	10.1	52.0	53.7	37.6	49.2	27.9	43.2
CSx3	61.7	8.7	80.8	6.5	84.2	81.3	70.0	13.1	65.3	73.7
CSx4	–	–	–	–	65.6	59.1	62.0	61.2	–	–
CSy1	–	–	67.2	14.4	67.3	82.1	62.6	84.9	62.6	85.8
CSy2	–	–	68.7	14.8	74.9	92.1	58.2	82.4	56.1	88.8
CSz1	20.2	2.3	16.4	0.1	19.5	0.2	18.1	0.1	21.8	6.2
CSz2	–	–	–	–	67.8	80.4	60.6	84.4	61.7	85.0

[a] All structures are geometry optimized and have ZPE corrections calculated at the levels indicated: B3LYP = B3LYP/6-311++G(2d,2p); MP2 = MP2/6-311++G(2d,2p). All energy values are given in kJmol^{-1}. [b] Single-point energies are calculated at the MP2/6-311++G(2d,2p)// B3LYP/6-311++G(2d,2p) level. All energy values are given in kJ mol^{-1}.

molecules from entering the drift tube. Ions drifted through the 2-m tube under the influence of a uniform electric field (5−25 V/cm) in helium buffer gas at pressures of 11−14 Torr. Following the drift tube the ion packet was collected by an exit ion funnel. The ions then were analyzed by a quadrupole mass filter and detected with a conversion dynode and electron multiplier.

Under the conditions used ions drift at a constant velocity, v_d, proportional to the applied field E

$$v_d = KE \tag{2}$$

The proportionality constant, K, is termed the ion mobility. By measuring the ion signal as a function of the arrival time t_a at the detector, an accurate value of K can be determined. Kinetic theory[34] relates K and thus t_a to the ion-helium collision cross section σ

$$\sigma = 1.3\left(\frac{q^2E^2T}{\mu k_B p^2 N^2 l^2}\right)^{1/2}(t_a - t_0) \tag{3}$$

where q is the ion charge, T the bath gas temperature averaged over the nine drift tube sections, p the tube pressure, μ the reduced mass of the ion-He collision partner, N the He gas density at 273 K and 760 Torr, k_B the Boltzmann constant, and l the length of the drift tube. The amount of time the ions spend outside the drift tube, t_0, is determined from data obtained at different drift voltages.[35] All the parameters on the right-hand side of eq 3 are known or can be measured accurately. Therefore, a precise value of σ can be obtained.

Computational Modeling. For the calculations, CS and SB structures of potassiated molecules (Scheme 2) were taken as input structures for a mixed low mode/Monte Carlo multiple minimum conformational search by using MacroModel 8.1 (Schrodinger Inc., Portland, OR). The conformational search was performed in 5000 steps, each followed by minimization using the Merck molecular force field (MMFF94s). Candidate structures with low MMFF energy were selected for higher level calculations.

B3LYP computations used the 6-311++G(2d,2p) basis set on all atoms as implemented in Gaussian 03.[36] Harmonic frequency calculations verified that all structures corresponded to local minima on the potential energy surface (PES) and provided zero-point energy (ZPE). Frequencies are scaled by a factor of 0.98 as found to be best suited for the level of theory applied.[37] For comparison to experiment, calculated vibrational frequencies are convoluted using a 20 cm^{-1} fwhm Gaussian line shape. To determine whether relative B3LYP energies agreed with more costly perturbation theory-based computations, optimization calculations at the MP2 level of theory (6-311++G(2d,2p)) were computed for all B3LYP structures. B3LYP and MP2 energies including ZPE corrections of all optimized geometries are given in Tables 1 and 2. All gas-phase ion structures are generated with GView 4.1 and depicted as ball and stick models.[36] We note that in these illustrations the

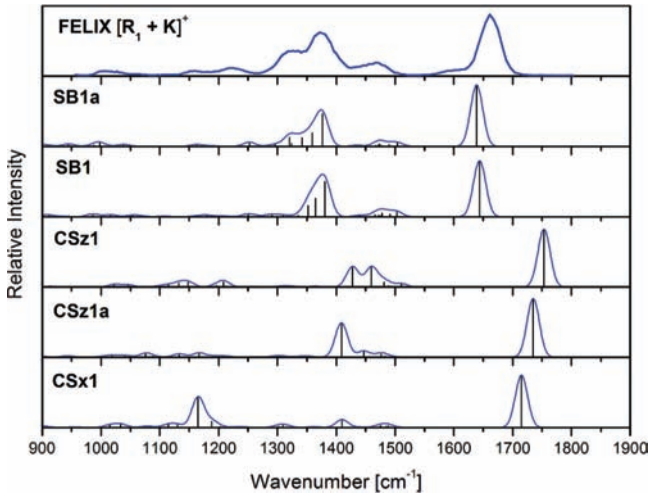

Figure 2. IRMPD spectrum of potassiated *N*-methyl proline $[R_1 + K]^+$ and calculated absorption spectra for the five most stable SB and CS isomers (B3LYP/6-311++G(2d,2p); Figure 3). Scaling factor 0.98.[37]

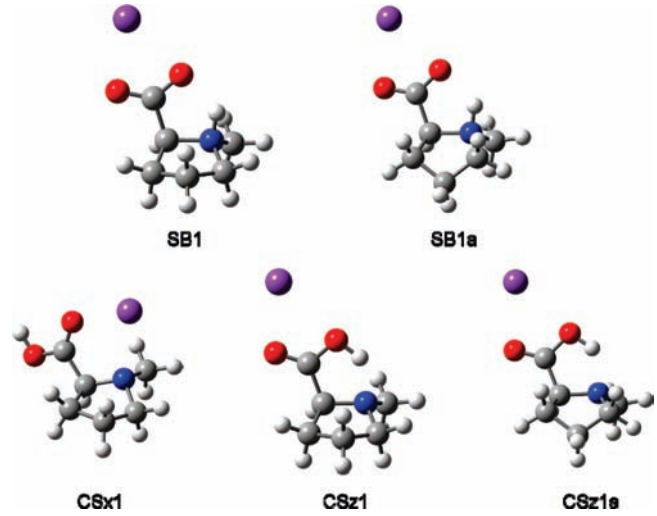

Figure 3. Five most stable structures of potassiated *N*-methyl proline $[R_1 + K]^+$ calculated at the B3LYP/6-311++G(2d,2p) level of theory (relative energies are listed in Table 1). Potassium is depicted in purple, nitrogen in blue, and oxygen in red.

size of the potassium cation K^+ is slightly too small in relation to the size of nitrogen, oxygen, hydrogen and carbon atoms.

Results and Discussion

Photo Dissociation Spectroscopy of Cyclic *N*-Methyl Amino Acids. The IRMPD spectra of the cyclic *N*-methyl amino acids $[R_n + K]^+$ with $n = 0-2$ are shown in Figure 1. The striking similarity of all three spectra suggests the presence of closely related conformers of the potassiated precursor ions examined. The spectra exhibit a set of three major signals at around 1650, 1380, and 1300 cm^{-1} (see spectrum of $[R_0 + K]^+$ Figure 1). With increasing ring size the latter absorption shifts to the blue and interferes with the neighboring band at 1380 cm^{-1} (1325 cm^{-1} $[R_1 + K]^+$, 1350 cm^{-1} $[R_2 + K]^+$). Additionally, two minor bands are detected at around 1460 cm^{-1} and near 1600 cm^{-1}.

In Figure 2, the IRMPD spectrum of *N*-methyl proline $[R_1 + K]^+$ is compared to calculated IR spectra of the lowest energy CS and SB conformers identified by theory (see Figure 3 and Table 1). All major features of the IRMPD spectrum of $[R_1 + K]^+$ are consistent with the spectra calculated for both relevant salt bridge structures SB1 and SB1a. The antisymmetric OCO stretch of the carboxylate moiety of the salt bridge structures SB1 and SB1a (calculated to be around 1640 cm^{-1}) is in very good agreement with the major band found at about 1660 cm^{-1} in the IRMPD spectrum of *N*-methyl proline $[R_1 + K]^+$. The significant signal at 1300 cm^{-1} in the spectrum of $[R_0 + K]^+$ (see Figure 1), at 1325 cm^{-1} in the spectrum of $[R_1 + K]^+$, and at 1350 cm^{-1} in the spectrum of $[R_2 + K]^+$ (see Figure 3S), which seems to be ring size dependent, is difficult to attribute to an individual absorption as shown in Figure 2 for the $[R_1 + K]^+$ ion. In fact multiple vibrations contribute to this band, including N−H and ring skeleton vibrations, which explains the ring size dependence of the band.

As Figure 3 illustrates the salt bridge structures SB1 and SB1a of $[R_1 + K]^+$ differ only in the folding of the pyrrolidine heterocycle. The SB1 structure is predicted to be the most stable conformer for $[R_1 + K]^+$ and $[R_2 + K]^+$ as suggested by MP2 calculations (Table 1). For both potassiated molecular ions, the closely related SB1a structure is favored by B3LYP by minor energy differences ($[R_1 + K]^+$, 4.5 $kJmol^{-1}$; $[R_2 + K]^+$, 0.9 $kJmol^{-1}$).

The four-membered azetidine ring of R_0 with its increased ring strain prevents extensive ring folding (Figure 2S of Supporting Information). In postassiated R_0 the position of the *N*-methyl group relative to the carboxylate determines the stability of the gas-phase structures. For $[R_0 + K]^+$ only one salt bridge conformer is competitive (SB1). B3LYP and MP2 predict uniformly that the SB structure of $[R_0 + K]^+$ is the most stable structure in the gas phase (Table 1; Figure 2S of Supporting Information). The IRMPD spectrum of $[R_0 + K]^+$ is compared to calculated spectra of respective SB and CS structures in Figure 1S of Supporting Information.

In potassiated *N*-methyl pipecolic acid $[R_2 + K]^+$ B3LYP and MP2 predict two salt bridge structures to be nearly equally stable, i.e., SB1 and SB1a (Table 1; Figure 4S of Supporting Information). All relevant SB structures of $[R_2 + K]^+$ are boat conformers of the six-membered piperidine ring mainly differing in the orientation of the methyl group at the ring nitrogen (Figure 4S of Supporting Information). The IRMPD spectrum of $[R_2 + K]^+$ is compared to calculated spectra of respective SB and CS structures in Figure 3S of Supporting Information.

For all three potassiated molecular ions $[R_n + K]^+$ salt bridge structures are energetically favored and the respective calculated IR spectra of these gas-phase ion structures match the recorded IRMPD spectra substantially better than the spectra of any CS structure.

The only unsatisfying aspect of the overall convincing structure assignment is related to the feature near 1600 cm^{-1}, which is stronger for R_0 and R_2 than for R_1 (Figure 1). This band finds no counterpart in the calculated spectra of either SB or CS ion structures of the $[R_n + K]^+$ ions identified by the theoretical models applied (Figures 1S−3S of Supporting Information). Possibly, the feature near 1600 cm^{-1} is due to a combination or overtone band that borrows intensity from the intense and nearby CO stretch mode. In addition, it is often observed in IRMPD spectroscopy that a weak band located slightly to the red of another (intense) band is enhanced due to the excitation process.[4]

Photodissociation Spectroscopy of Linear *N*-Methyl Amino Acids. Figure 4 shows the IRMPD spectra of the five linear tertiary amino acids as potassiated $[C_n + K]^+$ ions. The respective spectra exhibit characteristic absorptions at ~1375 cm^{-1}, at ~1475 cm^{-1}, and between 1600 and 1650 cm^{-1}. With

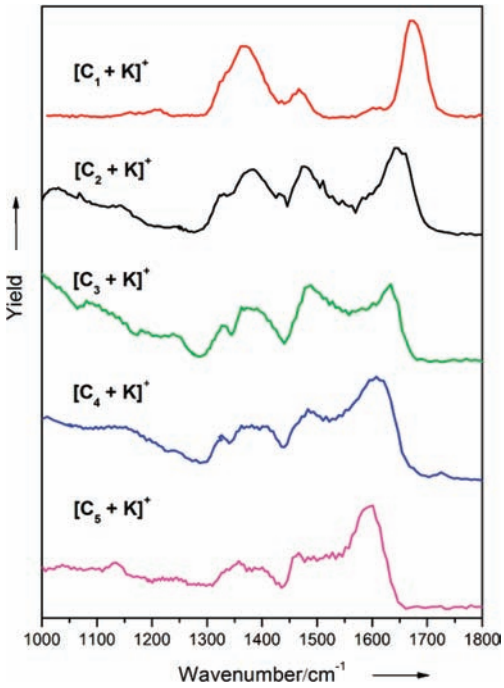

Figure 4. IRMPD spectra of the potassiated linear *N,N*-dimethyl amino acids $[C_n + K]^+$ ions with $n = 1-5$.

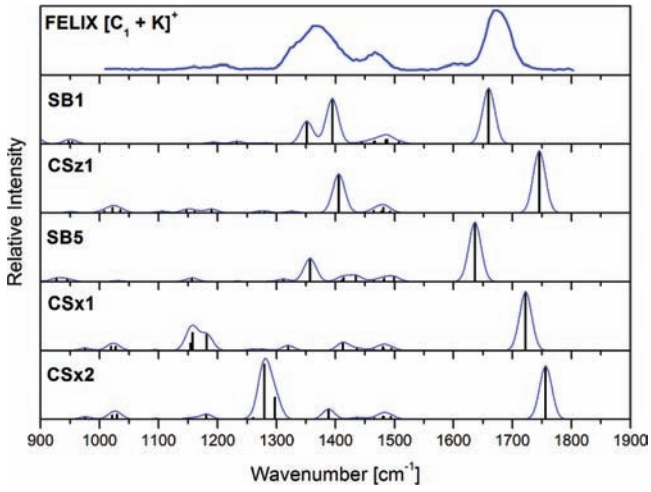

Figure 5. IRMPD spectrum of potassiated *N,N*-dimethyl glycine $[C_1 + K]^+$ and calculated spectra of the five most stable isomers. Scaling factor 0.98.[37]

longer alkyl chains of C_n ($n > 1$) the signals increasingly overlap. The major band at 1680 cm^{-1} shifts gradually to the red as the number of methylene groups n increases and interferes more and more with the band at 1475 cm^{-1}. Moreover, the spectral resolution of this set of IRMPD spectra is obviously gradually deteriorating.

Figure 5 shows the IRMPD spectrum of potassiated *N,N*-dimethyl glycine $[C_1 + K]^+$ in relation to calculated IR spectra for the most stable CS and SB conformers (see Figure 6). The best match with the experimental spectrum is found for the global minimum conformer SB1. Besides the good agreement of the bands in the 1300−1500 cm^{-1} region, the major absorption at ~1675 cm^{-1} corresponds nicely to the characteristic antisymmetric stretching mode of the carboxylate moiety.

As listed in Table 2, theory predicts for all five potassiated molecular ions $[C_n + K]^+$ similar salt bridge structures in the gas phase (SB1), in which the proton of the quarternary amine interacts with the carboxylic acid moiety. As the bandwidth of

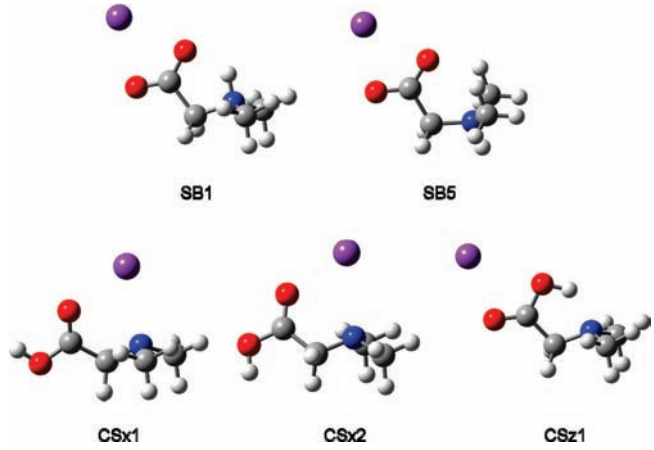

Figure 6. Five most stable structures of potassiated *N,N*-dimethyl glycine $[C_1 + K]^+$ complex ions calculated by B3LYP and MP2. Potassium is depicted in purple, nitrogen in blue, and oxygen in red.

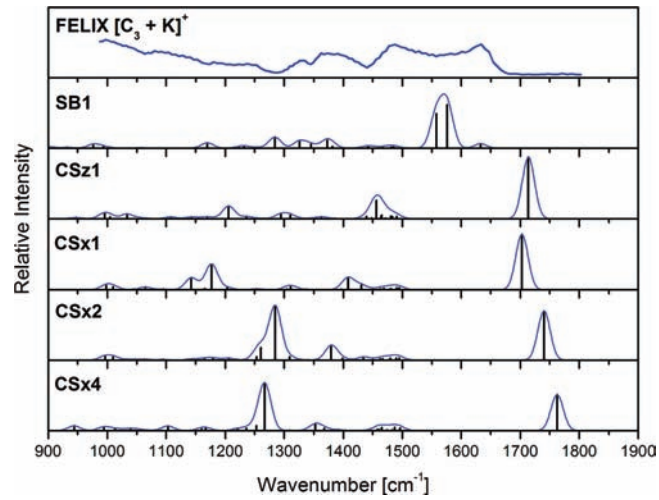

Figure 7. IRMPD spectrum of $[C_3 + K]^+$ and calculated spectra of the five most stable isomers. Scaling factor 0.98.[37]

the absorptions in the spectra of the $[C_n + K]^+$ ions increases for $n \geq 3$, the correlation with calculated IR spectra becomes more challenging (see Figure 7 for $[C_3 + K]^+$ and Figures 5S, 7S, and 9S of Supporting Information for $[C_n + K]^+$ with $n = 2, 4, 5$). However, the absence of an absorption band higher than 1680 cm^{-1}, where the fingerprint C═O stretching mode of the carboxylic acid group of charge solvated structures is predicted (e.g., CSz1 and CSxi structures, see Figure 8), suggests that CS structures do not occur for these ions. Despite substantially unresolved IRMPD spectra, the absence of this band clearly indicates that the linear $[C_n + K]^+$ ions ($n \geq 3$) adopt salt bridge structures in the gas phase. All relevant gas-phase conformers of the $[C_n + K]^+$ series of molecular ions are presented in Figure 6, 8, 6S, 8S, and 10S of Supporting Information.

The IRMPD spectrum of $[C_3 + K]^+$ presented in Figure 7 demonstrates the difficulties in assigning the experimental bands to the respective calculated IR spectra in the case of such unresolved absorption bands. Individual vibrational bands are hardly distinguishable. Moreover, vibrational frequencies calculated for the minimum energy structure of $[C_3 + K]^+$ provide at best a rough match; see for instance the two intense absorptions at around 1555 and 1570 cm^{-1}, which are attributed to coupled modes of the carboxylate CO stretch and the NH bend. To further investigate this, the features of the salt bridge structures of the $[C_n + K]^+$ ions are examined for characteristic

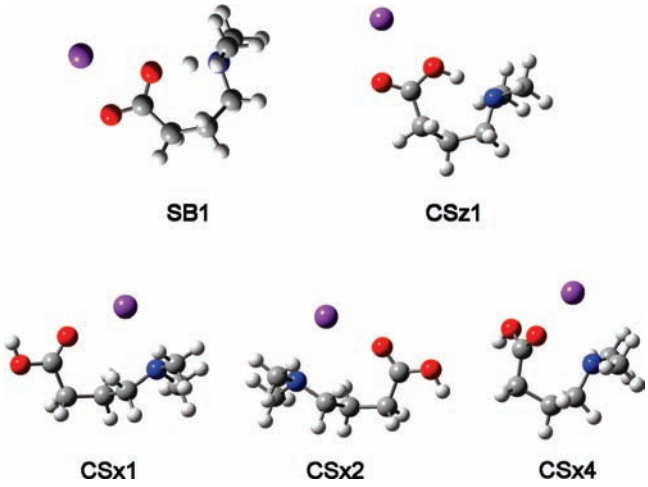

Figure 8. Five most stable structures of $[C_3 + K]^+$ complexes calculated at the B3LYP/6-311++G(2d,2p) level of theory. Potassium is depicted in purple, nitrogen in blue, and oxygen in red.

similarities and differences. This close-up reveals that all of the relevant SB structures exhibit a H-bonding interaction between the carboxylate oxygen and the proton on the amine group (e.g., see structure SB1 for $[C_3 + K]^+$ in Figure 8 and for $[C_n + K]^+$ Figures 6, 6S, 8S, and 10S of Supporting Information). This feature of all SB1 structures possibly explains the broadening in the IRMPD spectrum of, e.g., $[C_3 + K]^+$. Broad unresolved bands in IRMPD spectra are often encountered when a proton is shared between two heavy atoms (neutral or charged oxygens or nitrogens). Moreover, the absorption frequencies of these modes are hard to predict by harmonic calculations.[38−42] Instead of being close to harmonic, the PES experienced by the shared proton is relatively flat and anharmonic. In addition, the anharmonic nature of the vibrational modes involving the shared proton causes them to couple easily to other vibrational modes of the molecule.[38] A prominent example for this phenomenon is the IRMPD behavior of the protonated water dimer.[39] Generally, IRMPD spectra exhibit relatively broad spectral resonances, as compared to species not containing, e.g., an O···H$^+$···O moiety. To which extent the harmonic behavior of the proton is distorted depends on the degree of proton delocalization.[38] In the case of $[C_3 + K]^+$ ions a completely free oscillation of the proton is unlikely given the large energy gap (see Table 2) between SB1 and CSz1 structures, suggesting that the potential is still fairly asymmetric. However, it seems possible that an anharmonic motion of the proton adjacent to the carboxylate oxygen couples to the CO mode and is thereby responsible for the distorted absorption behavior.

Additionally, the H-bonding interaction between the carboxylate oxygen and the protonated amine in the SB structures of the $[C_n + K]^+$ ions offers an explanation for the gradual red shift of the major carboxylate CO stretching mode with increasing number of methylene groups n (Figure 4). The red shift of the carboxylate CO stretch mode indicates a decreasing CO bond strength, which is consistent with a stepwise strengthening of the H-bonding interaction between the carboxylate oxygen and the amine proton, which in turn rationalizes the decreasing spectral resolution. Hence, we conclude that the interaction of the carboxylate oxygen with the proton of the quarternary amine nitrogen strengthens as the methylene chain becomes longer and more flexible.

IMS. The experimentally measured cross sections for the series of potassiated teriary amino acid analytes $[C_n + K]^+$ and $[R_n + K]^+$ are shown in Figure 9 along with the cross sections

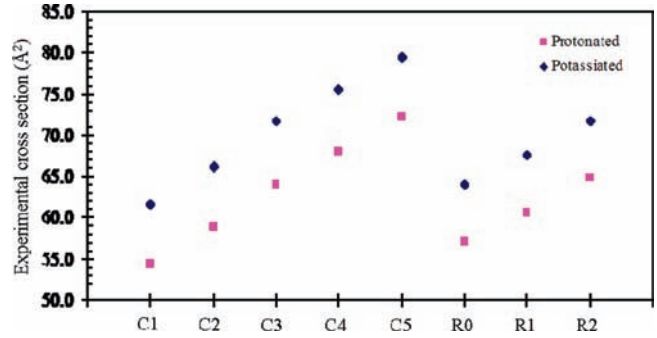

Figure 9. Experimentally measured collision cross sections for protonated and potassiated *N,N*-dimethyl amino carboxylic acids (C_n) and cyclic *N*-methyl amino acid analogues (R_n).

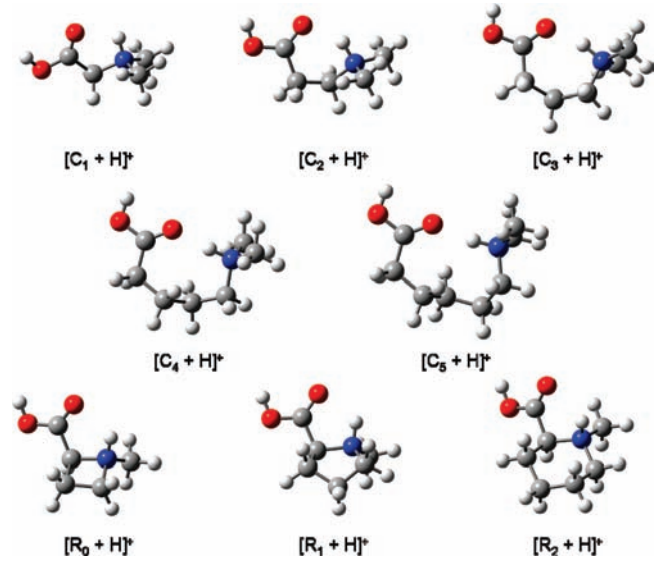

Figure 10. Structures of protonated *N,N*-dimethyl amino acids $[C_n + H]^+$ with $n = 1-5$ and cyclic *N*-methyl amino acids $[R_n + H]^+$ with $n = 0-2$.

for the corresponding protonated species $[C_n + H]^+$ and $[R_n + H]^+$. Since all of the protonated molecules assume a well-defined charge solvation structure with the additional proton always located at the nitrogen (see Figure 10), they are used as a reference to calibrate agreement between theory and experiment. Figure 9 indicates that the cross sections of both the protonated and potassiated systems increase monotonically with increasing system size, suggesting that the structures within one family of ions ($[C_n + H]^+$, $[R_n + H]^+$, $[C_n + K]^+$, and $[R_n + K]^+$) are of the same type (either CS or SB) regardless of n.

Figure 9 provides no evidence for a structural change occurring as a function of system size. Computationally, there are three families of structures (SB1, CSx1, and CSz1) found for the potassiated molecules (see Figures 3, 6, 8, and Figures 2S, 4S, 6S, 8S, and 10S of Supporting Information). Figure 11 indicates that all three families of potassiated structures agree about equally well with experiment. Calculated collision cross-section values[43,44] are slightly larger than experiment by 2−3 Å^2 for all molecular ions. However, if we take the data of the protonated molecular ions $[C_n + H]^+$ and $[R_n + H]^+$ shown in Figure 11A as calibration for the level of agreement expected between experiment and calculation, we conclude that the CSx1 data (Figure 11D) follow a slightly different pattern making the CSx structures less likely candidates. Calculated collision cross-section values of CSx structures are only ≤ 1 Å^2 larger than experimentally determined values. Both the SB1 and CSz1

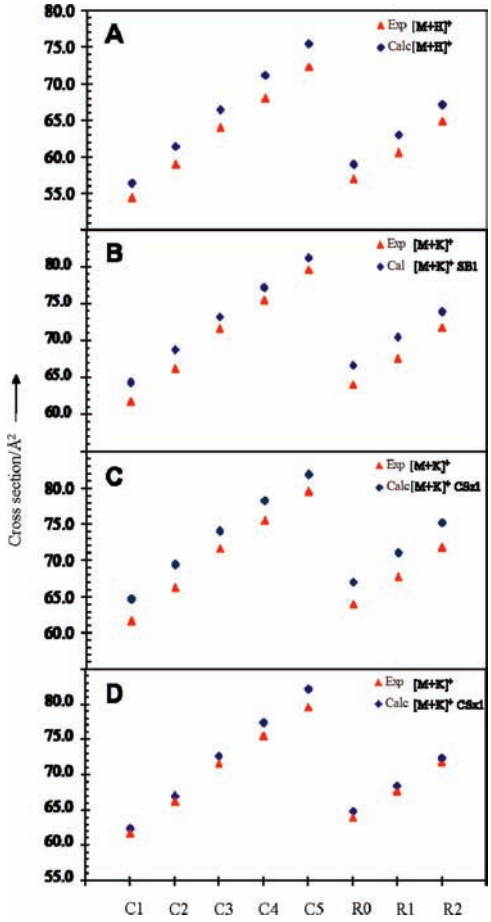

Figure 11. Experimentally measured and theoretically calculated cross sections for protonated and potassiated aminocarboxylic acids (C_n) and cyclic *N*-methyl amino acid analogues (R_n). (A) Protonated molecular ions $[M + H]^+$, (B) potassiated molecular ions $[M + K]^+$of the salt bridge structure SB1, (C) charge solvation structures CSz1, and (D) CSx1.

data (parts B and C of Figure 11) track the experimental trends equally well and in a fashion comparable to the $[M + H]^+$ data.

In conclusion, a preference of SB1 over CSz1 or vice versa is not possible on the basis of ion mobility data alone. However, experimental cross sections are in very good agreement with theoretical cross sections[43,44] evaluated for the lowest-energy SB structures of the potassiated species (Figure 11).

Conclusions

Our systematic gas-phase study of a series of potassiated tertiary amino acids yielded consistent structure assignments. The experimental IRMPD spectra of all potassiated tertiary amino acid molecules R_n and C_n correlate with the respective theoretical spectra calculated for their global minimum salt bridge structures, indicating that even the small potassiated molecular ion of *N,N*-dimethyl glycine adopts a salt-bridge structure in the gas phase. With increasing length and flexibility of the linear alkyl chain, the IRMPD spectral resolution degrades, making the correlation with calculated IR spectra less obvious. Although the increased conformational flexibility with increasing number of methylene groups *n* in the linear amino acids could be responsible for the observed spectral broadening, it seems more likely that anharmonic motions of the proton connected to the carboxylate oxygen and the amine nitrogen couples to the CO stretch mode and influences strongly the spectral habitus.

Collision cross-section measurements by ion mobility are consistent with the fact that all potassiated molecular ions studied adopt the same type of structure, i.e., an energetically favored salt bridge structure. However, IMS data alone cannot distinguish between the SB and CS structures for the set of potassiated ions examined. The resolution of IMS was found to be insufficient for a reliable assignment of either of these isomeric structures as the collision cross sections are only slightly different. Further systems are being designed and examined to refine the delicate competition between the intrinsic stabilities of SB and CS structural motifs.

The systematic study of an array of model amino acids may thus be useful to facilitate understanding of the fundamental relation between molecular structure and the tendency to form salt bridges in the gas phase, a topic of importance for the correct assignment of three-dimensional peptide and protein structures in solvent free environments.

Acknowledgment. Financial support by the "Nederlandse Organisatie voor Wetenschappelijk Onderzoek", the German research Foundation (DFG), and the National Science Foundation (U.S.A.) is acknowledged. Generous provision of computing power at the Regional Computing Centre RRZK, Cologne, Germany, and in the D-GRID initiative is gratefully acknowledged. The authors thank Frank Dreiocker, Department of Chemistry, University of Cologne, for providing all tertiary amino acid compounds and Dr. Britta Redlich for her skillful assistance at the FELIX facility.

Supporting Information Available: Figures depicting data as noted in the above text and complete reference 36. This material is available free of charge via the Internet at http://pubs.acs.org.

References and Notes

(1) von Helden, G.; Ming-Teh Hsu, M.-T.; Kemper, P. R.; Bowers, M. T. *J. Chem. Phys.* **1991**, *95*, 3835–3837.
(2) Wyttenbach, T.; Bowers, M. T. *Top. Curr. Chem.* **2003**, *225*, 207–232.
(3) Polfer, N.; Oomens, J. *Phys. Chem. Chem. Phys.* **2007**, *9*, 3804–3817.
(4) Oomens, J.; Sartakov, B. G.; Meijer, G.; von Helden, G. *Int. J. Mass Spectrom.* **2006**, *254*, 1–19.
(5) Moision, R. M.; Armentrout, P. B. *J. Phys. Chem. A* **2006**, *110*, 3933–3943.
(6) Tally, J. M.; Cerda, B. A.; Ohanessian, G.; Wesdemiotis, C. *Chem.—Eur. J.* **2002**, *8*, 1377–1388.
(7) Remko, M.; Fitz, D.; Rode, B. M. *J. Phys. Chem. A* **2008**, *112*, 7652–7661.
(8) Strittmatter, E. F.; Lemoff, A. S.; Williams, E. R. *J. Phys. Chem. A* **2000**, *104*, 9793–9796.
(9) Marino, T.; Russo, N.; Toscano, M. *J. Inorg. Biochem.* **2000**, *79*, 179–185.
(10) Forbes, M. W.; Bush, M. F.; Polfer, N.; Oomens, J.; Dunbar, R. C.; Williams, E. A.; Jockusch, R. A. *J. Phys. Chem. A* **2007**, *111*, 11759–11770.
(11) Bush, M. F.; Forbes, M. W.; Jockusch, R. A.; Oomens, J.; Polfer, N.; Saykally, R. J.; Williams, E. R. *J. Phys. Chem. A* **2007**, *111*, 7753–7760.
(12) Armentrout, P. B.; Rodgers, M. T.; Oomens, J.; Steill, J. D. *J. Phys. Chem. A* **2008**, *112*, 2258–2267.
(13) Rodgers, M. T.; Armentrout, P. B.; Oomens, J.; Steill, J. D. *J. Phys. Chem. A* **2008**, *112*, 2248–2251.
(14) Bush, M. F.; Oomens, J.; Saykally, J.; Williams, E. R. *J. Phys. Chem. A* **2008**, *112*, 8578–8584.
(15) Bush, M. F.; Oomens, J.; Saykally, R. J.; Williams, E. A. *J. Am. Chem. Soc.* **2008**, *130*, 6463–6471.
(16) Dunbar, R. C.; Polfer, N. C.; Oomens, J. *J. Am. Chem. Soc.* **2007**, *129*, 14562–14563.
(17) Wyttenbach, T.; Witt, M.; Bowers, M. T. *Int. J. Mass Spectrom.* **1999**, *182/183*, 243–252.
(18) Wyttenbach, T.; Witt, M.; Bowers, M. T. *J. Am. Chem. Soc.* **2000**, *122*, 3458–3464.

(19) Rajabi, K.; Fridgen, D. *J. Phys. Chem. A* **2008**, *112*, 23–30.
(20) Wu, R.; McMahon, T. B. *J. Am. Chem. Soc.* **2007**, *129*, 4864–4865.
(21) Polfer, N.; Paizs, B.; Snoek, L. C.; Compagnon, I.; Suhai, S.; Meijer, G.; von Helden, G.; Oomens, J. *J. Am. Chem. Soc.* **2005**, *127*, 8571–8579.
(22) Wyttenbach, T.; Bushnell, J. E.; Bowers, M. T. *J. Am. Chem. Soc.* **1998**, *120*, 5098–5103.
(23) Baumketner, A.; Bernstein, S. L.; Wyttenbach, T.; Lazo, N. D.; Teplow, D. B.; Bowers, M. T.; Shea, J.-E. *Protein Sci.* **2006**, *15*, 1239–1247.
(24) Wu, C.; Murray, M. M.; Bernstein, S. L.; Condron, M. M.; Bitan, G.; Shea, J.-E.; Bowers, M. T. *J. Mol. Biol.* **2009**, *387*, 492–501.
(25) Liu, D.; Seuthe, A. B.; Ehrler, O. T.; Zhang, X.; Wyttenbach, T.; Hsu, J. F.; Bowers, M. T. *J. Am. Chem. Soc.* **2005**, *127*, 2024–2052.
(26) Wyttenbach, T.; Liu, D.; Bowers, M. T. *J. Am. Chem. Soc.* **2008**, *130*, 5993–5995.
(27) Hunter, E. P.; Lias, S. G. *J. Phys. Chem. Ref. Data* **1998**, *27*, 413–656.
(28) Rahal, S.; Badache, L. *Tetrahedron Lett.* **1991**, *32*, 3847–3848.
(29) Aurelio, L.; Box, J. S.; Brownlee, R. T. C.; Huges, A. B.; Sleebs, M. M. *J. Org. Chem.* **2003**, *68*, 2652–2667.
(30) Valle, J. J.; Eyler, J. R.; Oomens, J.; Moore, D. T.; van der Meer, A. F. G.; von Helden, G.; Meijer, G.; Hendrickson, C. L.; Marshall, A. G.; Blakney, G. T. *Rev. Sci. Instrum.* **2005**, *76*, 023103.
(31) Polfer, N. C.; Oomens, J.; Moore, D. T.; von Helden, G.; Meijer, G.; Dunbar, R. C. *J. Am. Chem. Soc.* **2006**, *128*, 517–525.
(32) Oepts, D.; van der Meer, A. F. G.; van Amersfoort, P. W. *Infrared Phys. Technol.* **1995**, *36*, 297–308.
(33) Kemper, P. R.; Dupuis, N. F.; Bowers, M. T. Int. J. Mass Spectrom. 2009, in press.
(34) Mason, E. A.; McDaniel, E. W. *Transport Properties of Ions in Gases*; Wiley, New York, NY, 1988.
(35) Kemper, P. R.; Bowers, M. T. *J. Phys. Chem.* **1991**, *95*, 5134–5146.
(36) Frisch, M. J.; Trucks, G. W.; Schlegel, H. B.; Scuseria, G. E.; Robb, M. A.; Cheeseman, J. R.; Montgomery, J. A., Jr.; Vreven, T.; Kudin, K. N.; Burant, J. C.; Millam, J. M.; Iyengar, S. S.; Tomasi, J.; Barone, V.; Mennucci, B.; Cossi, M.; Scalmani, G.; Rega, N.; Petersson, G. A.; Nakatsuji, H.; Hada, M.; Ehara, M.; Toyota, K.; Fukuda, R.; Hasegawa, J.; Ishida, M.; Nakajima, T.; Honda, Y.; Kitao, O.; Nakai, H.; Klene, M.; Li, X.; Knox, J. E.; Hratchian, H. P.; Cross, J. B.; Bakken, V.; Adamo, C.; Jaramillo, J.; Gomperts, R.; Stratmann, R. E.; Yazyev, O.; Austin, A. J.; Cammi, R.; Pomelli, C.; Ochterski, J. W.; Ayala, P. Y.; Morokuma, K.; Voth, G. A.; Salvador, P.; Dannenberg, J. J.; Zakrzewski, V. G.; Dapprich, S.; Daniels, A. D.; Strain, M. C.; Farkas, O.; Malick, D. K.; Rabuck, A. D.; Raghavachari, K.; Foresman, J. B.; Ortiz, J. V.; Cui, Q.; Baboul, A. G.; Clifford, S.; Cioslowski, J.; Stefanov, B. B.; Liu, G.; Liashenko, A.; Piskorz, P.; Komaromi, I.; Martin, R. L.; Fox, D. J.; Keith, T.; Al-Laham, M. A.; Peng, C. Y.; Nanayakkara, A.; Challacombe, M.; Gill, P. M. W.; Johnson, B.; Chen, W.; Wong, M. W.; Gonzalez, C.; Pople, J. A. *Gaussian 03*, revision D.01; Gaussian, Inc.: Wallingford, CT, 2004.
(37) Polfer, N.; Oomens, J.; Dunbar, R. C. *Phys. Chem. Chem. Phys.* **2006**, *8*, 2744–2751.
(38) Oomens, J.; Steill, J. D.; Redlich, B. *J. Am. Chem. Soc.* **2009**, *131*, 4310–4319.
(39) Asmis, K. R.; Pivonka, N. L.; Santambrogio, G.; Brümmer, M.; Kaposta, C.; Neumark, D. M.; Wöste, L. *Science* **2003**, *299*, 1375–1377.
(40) Moore, D. T.; Oomens, J.; van der Meer, L.; von Helden, G.; Meijer, G.; Valle, J.; Marshall, A. G.; Eyler, J. R. *Chem. Phys. Chem.* **2004**, *5*, 740–743.
(41) Fridgen, T. D.; McMahon, T. B.; MacAleese, L.; Lemaire, J.; Maitre, P. *J. Phys. Chem. A* **2004**, *108*, 9008–9010.
(42) Fridgen, T. D.; MacAleese, L.; Maitre, P.; McMahon, T. B.; Boissel, P.; Lemaire, J. *Phys. Chem. Chem. Phys.* **2005**, *7*, 2747–2755.
(43) Wyttenbach, T.; von Helden, G.; Batka Jr, J. J.; Carlat, D.; Bowers, M. T. *J. Am. Soc. Mass Spectrom.* **1997**, *8*, 275–282.
(44) von Helden, G.; Hsu, M.-T.; Gotts, N.; Bowers, M. T. *J. Phys. Chem.* **1993**, *97*, 8182–8192.

JP903036T